Supplement of

Optimizing a twin-chamber system for direct ozone production rate measurement

Yaru Wang[1#], Yi Chen[2#], Suzhen Chi[1#], Jianshu Wang[1], Chong Zhang[1], Weixiong Zhao[3], Weili Lin[2], Chunxiang Ye[1*]

[1]State Key Joint Laboratory for Environmental Simulation and Pollution Control, Center for Environment and Health, and College of Environmental Sciences and Engineering, Peking University, Beijing, 100871, China.
[2]Key Laboratory of Ecology and Environment in Minority Areas (Minzu University of China), National Ethnic Affairs Commission, Beijing, 100081, China.
[3]Laboratory of Atmospheric Physico-Chemistry, Chinese Academy of Sciences Hefei Institutes of Physical Science Anhui Institute of Optics and Fine Mechanics, Chinese Academy of Sciences, Hefei, 230031, Anhui, China.

[#]Yaru Wang, Yi Chen and Suzhen Chi contribute equally to this work.

[*]*Correspondence to*: Chunxiang Ye (c.ye@pku.edu.cn)

S1. Design of Mea-OPR system

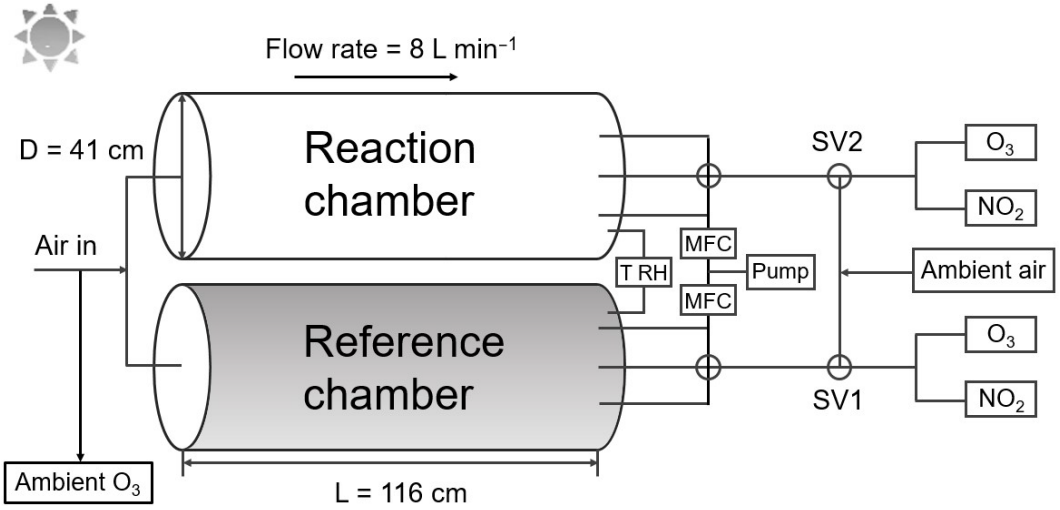

Figure S1: Schematic of ozone production rate measurement system, Mea-OPR. SV: solenoid valve. MFC: mass flow controller.

Design improvement of Mea-OPR system has lower O_3 uptake coefficient of 8.12×10^{-9}, relative to 7.11×10^{-8} in quartz chambers (Sklaveniti et al., 2018). Mea-OPR also has smaller S/V ratio (9.8 m^{-1}) compared to the smallest value published in literature, 18 m^{-1} (Baier et al., 2015). Both help to reduce O_x uptake. Meanwhile, Mea-OPR has more flexible flow rate range (5–20 L min^{-1}) owing to its larger volume (153 L) relative to the largest value (26.9 L) published in literature (Baier et al., 2015). Moreover, Mea-OPR has longer residence time (up to 30 min) compared to the longest value of 20.5 min published in literature (Sadanaga et al., 2017).

S2. Characterization of Mea-OPR system

S2.1 Photochemical conditions in both chambers

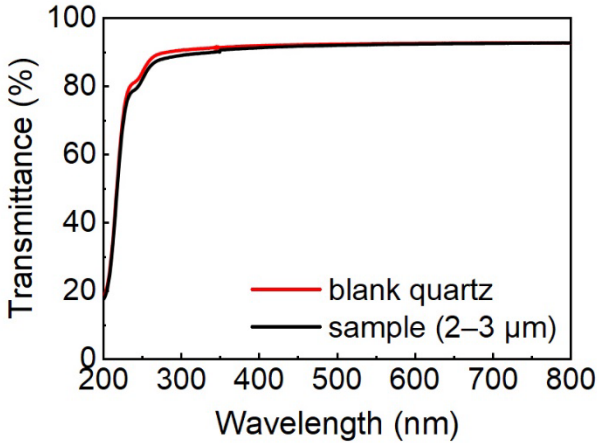

Figure S2: Detected light transmittances for blank quartz and quartz flakes coated with 2–3 μm thick Teflon film (as indicated by sample). For light with wavelength above 290 nm, light transmittance of blank and Teflon-coated quartz could reach above 88%.

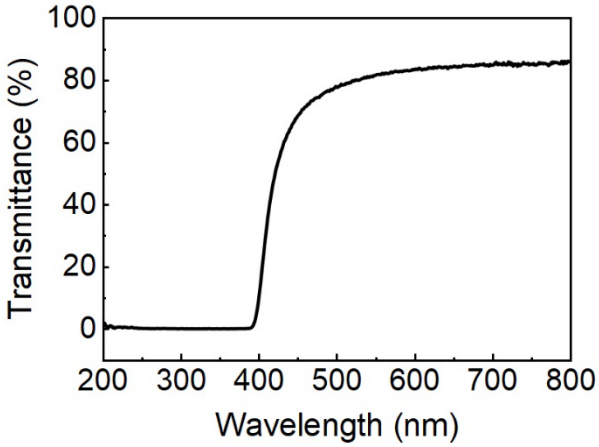

Figure S3: Light transmittance of UV filter film (PEI, 0.25 mm thick). Light transmittance is less than 50% at wavelength below 420 nm and approximately zero at wavelength below 390 nm.

Table S1. Comparison of photolysis rate constants of different species in the ambient, reaction chamber, and reference chamber.

	Ambient	Reaction	Reference	Rea/Amb	Ref/Amb
$j(NO_2)$	7.55×10^{-3}	7.16×10^{-3}	2.79×10^{-4}	0.95	0.04
$j(O^1D)$	1.31×10^{-5}	1.26×10^{-5}	6.75×10^{-7}	0.96	0.05
j(HONO)	1.28×10^{-3}	1.21×10^{-3}	3.98×10^{-5}	0.95	0.03
j(HCHO_M)	3.39×10^{-5}	3.20×10^{-5}	1.09×10^{-6}	0.94	0.03
j(HCHO_R)	2.17×10^{-5}	2.05×10^{-5}	8.07×10^{-7}	0.95	0.04
$j(NO_3$_M)	1.86×10^{-2}	1.78×10^{-2}	1.09×10^{-2}	0.96	0.59
$j(NO_3$_R)	1.53×10^{-1}	1.46×10^{-1}	7.86×10^{-2}	0.96	0.51

As shown by the data listed in Table S1, $j(O^1D)$ in the reaction chamber is greater than 96% of the ambient value, and $j(O^1D)$ in the reference chamber is less than 5% of the ambient value. These results show that the reaction chamber can simulate the photochemical process of O_3 ideally, while the reference chamber can suppress it.

S2.2 Temperature and relative humidity in both chambers

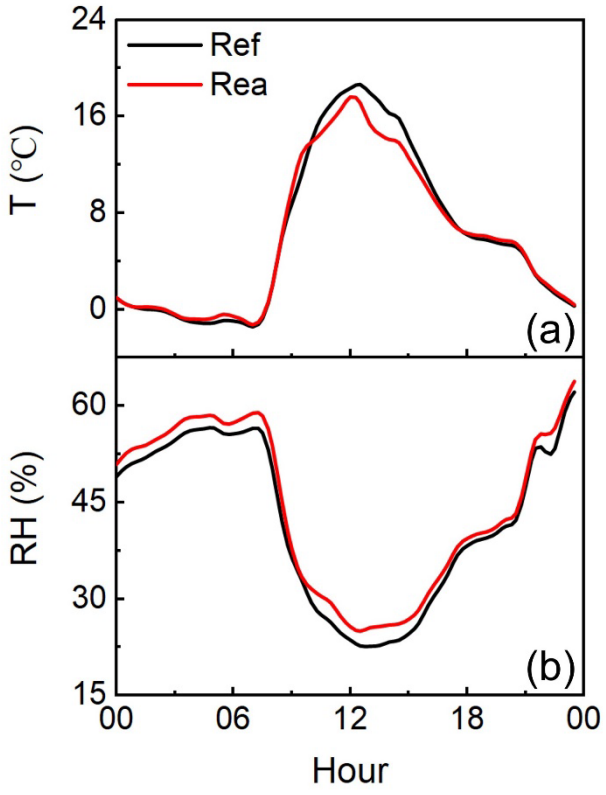

Figure S4: Similar (a) temperature and (b) RH conditions in reaction and reference chambers on 11 February, 2022.

S2.3 Regular calibrations for O_3 and NO_2 analyzers

The O_3 and NO_2 analyzers were regularly (every two weeks) calibrated using NO_2 (produced by gas-phase titration using NO and O_3) and O_3 (generated by O_3 calibrator, Thermo Scientific, Model 49i-PS) standard gases during the field campaign and the calibrations suggested that the slope changes were less than ±0.4% in O_3 analyzers and ±1.9% in NO_2 analyzers (Table S2), suggesting the good stability of measurement signals for analyzers.

Table S2. Calibration curves for three O_3 analyzers and three NO_2 analyzers during field campaign.

	Slope	Intercept	R^2
O_3_ref	1.01 (±0.004)	0.62 (±0.047)	1
O_3_rea	1.00 (±0.002)	−0.13 (±0.080)	1
O_3_amb	0.98 (±0.001)	1.60 (±0.032)	1
NO_2_ref*	0.75 (±0.014)		0.998
NO_2_rea*	0.78 (±0.008)		0.998
NO_2_amb*	–	–	–

*Default intercept of LGR calibration curves is 0. NO_2_amb was measured by iBBCES-NO_2, which is absolute measuring instrument and does not require calibration.

S2.4 Consistency checks for O_3 and NO_2 between analyzers

Notably, in addition to the analyzer calibrations, parallel measurements using two sets of analyzers showed some deviation, which raised uncertainties in ΔO_3 and ΔNO_2 measurements. The consistency was checked daily under dark conditions from 22:00 to 23:00 with O_3 and NO_2 analyzers directly measuring ambient air through the solenoid valve switch. The measured data were compared with the real-time ambient values obtained from the other two on-line continuous O_3 and NO_2 analyzers. After 1 month of field observation, the measured average half-hour O_3 (NO_2) data in both chambers and the ambient air showed fairly good agreement ($R^2 = 1$). The difference values between two parallel analyzers during consistency measurements are shown in Fig. S5. The difference values between two O_3 and two NO_2 analyzers, ΔO_3 and ΔNO_2, are within the range of ±0.4 ppbv, within the instrument detection limits, indicating that the parallel measurement is reliable.

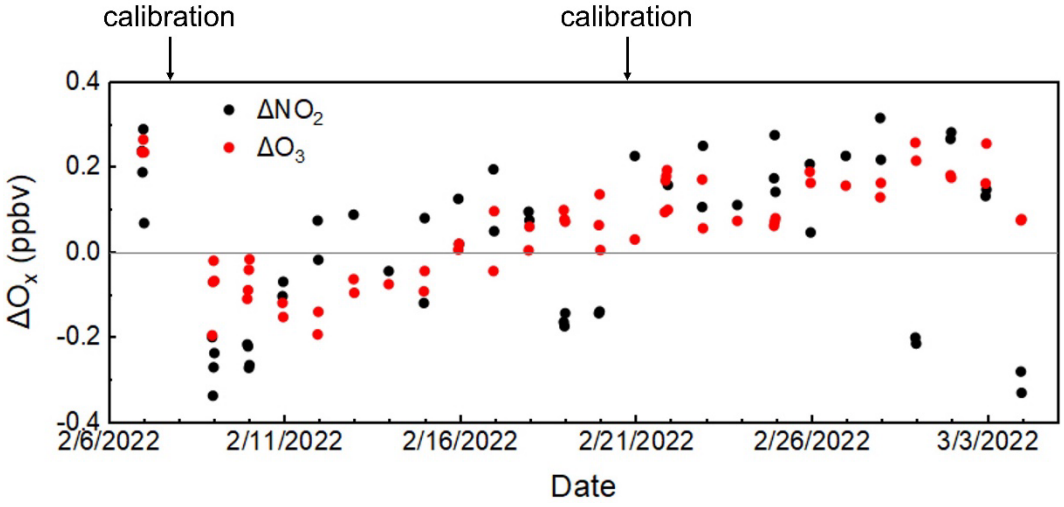

Figure S5: Difference values of O_3 and NO_2 between two parallel analyzers, ΔO_3 and ΔNO_2, during consistency measurements. Two calibration tests were conducted on 7 and 20 February, 2022.

S2.5 Determination of gas residence time in chambers

As the chamber volume and air sampling rate are 153 L and 8 L min^{-1}, respectively, the theoretically calculated τ is 19.1 min assuming completely ideal laminar flow. The experiments to determine real τ were performed by introducing a short pulse of CO standard gas at the inlet. The percentage change of CO concentrations at the exit is shown in Fig. S6. The real τ could be obtained according to Eq. (S1) and (S2) (Sadanaga et al., 2017). The mean τ calculated for the reaction (τ_Rea) and reference (τ_Ref) chambers are 19.7 (±0.07) min and 20.2 (±0.05) min, respectively. The average of both τ is 19.9 (±0.09) min, which approximates the theoretical τ (19.1 min), indicating the air passing the chambers can be treated as an approaching laminar flow.

$$E(\tau) = \frac{C(\tau)}{\int_0^\infty C(\tau)\, d\tau} \quad \text{(S1)}$$

$$\tau = \int_0^\infty \tau\, E(\tau)\, d\tau \quad \text{(S2)}$$

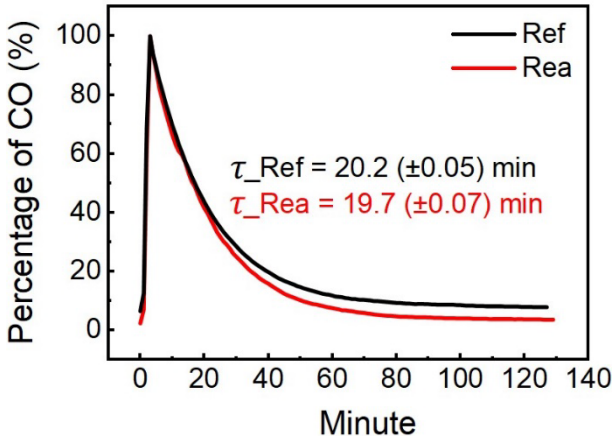

Figure S6: Percentage change of CO concentrations during residence time experiments.

S2.6 Condition experiments to characterize wall effect

During the zero-NO_x-and-high-O_3 experiment, a high concentration of O_3 (1 ppmv) of approximately 2.5 L min^{-1} was produced by an O_3 generator (Thermo Scientific, Model 49i-PS) and diluted by zero air to reach the overall flow rate of 17.5 L min^{-1} and O_3 concentration of 113.0 ppbv before entering both chambers. In addition to O_3 and NO_2, measurements of NO (Thermo Scientific, Model 42i), CO (Thermo Scientific, Model 48i) and HONO (long-path absorption photometer, LOPAP, homemade) in the chambers were also equipped during the control experiment. 0.5 ppmv CO (impurity in the zero air) and 1.05 ppbv NO_x (chamber source of NO_x (Zhou et al., 2003)) were still observed in the reaction chamber, so that O_3 photochemical production in the reaction chamber was double-checked using a photochemical box model based on the Master Chemical Mechanism (Saunders et al., 2003). Small production of O_3 in the reaction chamber in the control experiment could be quantified and corrected, so that O_3 uptake loss, $\Delta O_{3,\,uptake}$, can be obtained from the differential O_3 between the inlet and outlet of each chamber.

Uptake coefficient of O_3 on the wall (γ_{O3}) was then calculated in Eq. (4). Further, the uptake coefficient was associated with $j(O^1D)$ in the daytime and RH at night, and the corresponding relationship curve was fitted, which could be used to correct the O_3 uptake loss difference between both chambers as Mea-OPR was deployed.

During the 1-week HONO production experiment, HONO in the ambient and both chambers were simultaneously measured using a customized homemade LOPAP, which is characterized by wet chemical sampling and photometric detection. The detailed description of LOPAP can be found in Wang et al.(2023). Comprehensive ambient parameters concerning O_3 photochemistry, including *j* values (Metcon CCD-Spectrograph), CO (Thermo Scientific, Model 48i), NO (Thermo Scientific, Model 42i-Y), and VOCs and OVOCs (GC-MS, TH-PKU 300B, Wuhan Tianhong Instrument Co., Ltd., China), were luckily available during the 1-week HONO production experiment. Based on this, the perturbation of differential HONO between the reaction chamber and the ambient on OPR can then be evaluated using the MCM model.

During the 1-week HONO production experiment, the NO_x in the ambient and both chambers were measured simultaneously, and the NO_x difference between the ambient and the chamber was approximated as the NO_2 uptake loss, $\Delta NO_{2,\,uptake}$. Therefore, the NO_2 uptake coefficient in the chambers, γ_{NO_2}, can be calculated referring to Eq. (S3), wherein $NO_{2,\,amb}$ represents the ambient NO_2 concentration in ppbv. ω_{NO2} represents mean molecular velocity of NO_2 in m s^{-1}.

$$\gamma_{NO_2} = \frac{4 \times \Delta NO_{2,\,uptake}}{NO_{2,\,amb} \times \omega_{NO2} \times \tau \times S/V} \quad \text{(S3)}$$

Table S3. Comparison of uptake losses of O_3 and NO_2 on quartz and Teflon coating quartz surfaces. Notably, uptake coefficients of O_3 (γ_{O3}) and NO_2 (γ_{NO2}) were obtained using Eq. (4) and (S3), respectively. Reference data were from two recently published papers: Sklaveniti et al., 2018 and Sadanaga et al., 2017.

Material of chamber	Diameter (cm)	Length (cm)	Flow rate (L min^{-1})	Residence time (min)	γ_{O3}*	γ_{NO2}*	Reference
Quartz	14	70	2.25	4.52	7.11×10^{-8}	6.98×10^{-8}	(Sklaveniti et al., 2018)
Quartz coated with Teflon	17.1	50	0.543	20.5	5.17×10^{-9}	8.09×10^{-9}	(Sadanaga et al., 2017)

*Uptake coefficients were measured under dark conditions.

MCM model construction

O_3 production in above zero-NO_x-and-high-O_3 experiment and the O_3 production difference between the reaction chamber and the ambient from the 1-week HONO production experiment can be simulated using the MCM model. In the zero-NO_x-and-high-O_3 experiment, the model was constrained with the measured parameters concerning O_3 photochemistry, including CO, HONO, O_3, NO, NO_2, *j* values, temperature and H_2O. Only 48 gas-phase inorganic reactions extracted from the website of Leeds University (MCM v3.3.1, http://mcm.leeds.ac.uk/MCM) were included in the chemical mechanism to mimic the O_3 photochemistry in the zero air. The time resolution was set as 15 min in the MCM model. Photochemical production rate of O_3 in reaction chamber by MCM simulation during condition experiment of O_3 uptake is shown in Fig. S7.

To simulate O_3 photochemistry in the 1-week HONO production experiment, our preliminary model was constrained by measurements of CO, HONO, O_3, NO, NO_2, *j* values, temperature, H_2O, and individual VOC/OVOC species measured using GC-MS at a 1-hour time resolution. For the MCM model, the time resolution was set at 1 h. The preliminary model showed that the sum of k_{OH} contributed by NO_x, O_3, CO, VOCs, OVOCs, and model intermediates was less than the measured k_{OH} (LFP-FRS, AIOFM), i.e., k_{OH} was missing. The detailed description of k_{OH} measurement can be found in Wei et al.(2020). An additional formaldehyde (HCHO) and thus HCHO+OH reaction was further included in our box model to represent the missing k_{OH}. Based on such simulation, O_3 production in the ambient and the reaction chamber can be calculated and compared.

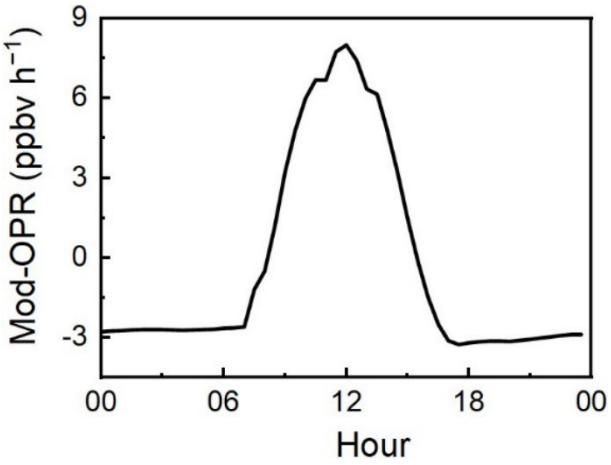

Figure S7: Photochemical production rate of O_3 in reaction chamber by MCM simulation during condition experiment of O_3 uptake.

S2.7 Uncertainty calculation of Mea-OPR

Mea-OPR can be calculated by Eq. (5).

For several calibrations of O_3 analyzers, the slope changes were less than ±0.4%, suggesting the good stability of O_3 measurement. Therefore, we do not consider the uncertainty of $O_{3,\,amb}$ in Eq. (5). Similarly, because the uncertainty was less than ±1% in the temperature measurement, we do not consider the uncertainty of ω calculated thereby. D is a constant, 0.41 m.

1. During the consistency measurement, the ratio of ΔNO_2 to NO_2, X_{NO_2}, was relatively constant at high concentrations. Based on this ratio, the $\Delta NO_{2,\,inconsistent}$ caused by the inconsistency between both analyzers during Mea-OPR measurement can be obtained. $\Delta NO_{2,\,inconsistent}$ is just the absolute uncertainty of ΔNO_2, $\delta\Delta NO_2$. Thus, the uncertainty of the ΔNO_2 measurements can be obtained (Eq. S6). Similarly, the uncertainty of ΔO_3 measurements can be calculated (Eq. S9). When NO_2 is above 10 ppbv, X_{NO_2} remains constant, and the average value is 0.40%. When O_3 is above 5 ppbv, X_{O_3} is equal to 0.17%. Notably, NO_2 and O_3 are uniformly referred to as the NO_2 and O_3 concentrations in the reference chamber.

$$\Delta NO_2 = NO_{2,\,Rea} - NO_{2,\,Ref} \quad \text{(S4)}$$

$$\delta\Delta NO_2 = \Delta NO_{2,\,inconsistent} = NO_{2,\,Ref} \cdot X_{NO_2} \quad \text{(S5)}$$

$$Unc_{\Delta NO_2} = \frac{\delta\Delta NO_2}{\Delta NO_2} \quad \text{(S6)}$$

$$\Delta O_3 = O_{3,\,Rea} - O_{3,\,Ref} \quad \text{(S7)}$$

$$\delta\Delta O_3 = \Delta O_{3,\,inconsistent} = O_{3,\,Ref} \cdot X_{O_3} \quad \text{(S8)}$$

$$Unc_{\Delta O_3} = \frac{\delta\Delta O_3}{\Delta O_3} \quad \text{(S9)}$$

2. The results of the gas residence time experiments revealed that the mean gas residence time (τ) in the chambers was 19.9 ($\pm$0.09, $\delta\tau$) min and that the relative uncertainty was $\pm$0.45% (Eq. S10).

$$\mathrm{Unc}_{\tau} = \frac{\delta\tau}{\tau} = \frac{0.09}{19.9} = 0.45\% \quad \text{(S10)}$$

3. According to the O_3 uptake experiment, the fitting relation between γ_{O3} in both chambers and $j(O^1D)$ were obtained (Eq. S11 and S12). Statistically, the fitting parameters have certain uncertainty, and the uncertainty of γ_{O3} obtained thereby can be calculated using Eqs. (S13)–(S16).

$$\gamma_{\mathrm{Ref}} = a_1 \times \exp\left(-\frac{j(O^1D)}{b_1}\right) + c_1 \quad \text{(S11)}$$

where a_1 ($\pm\delta a_1$) = -5.53×10^{-9} ($\pm 4.83 \times 10^{-10}$), b_1 ($\pm\delta b_1$) = 5.41×10^{-6} ($\pm 1.51 \times 10^{-6}$), c_1 ($\pm\delta c_1$) = 1.96×10^{-8} ($\pm 5.50 \times 10^{-10}$).

$$\gamma_{\mathrm{Rea}} = a_2 \times \exp\left(-\frac{j(O^1D)}{b_2}\right) + c_2 \quad \text{(S12)}$$

where a_2 ($\pm\delta a_2$) = -8.21×10^{-8} ($\pm 7.56 \times 10^{-9}$), b_2 ($\pm\delta b_2$) = 9.76×10^{-6} ($\pm 2.12 \times 10^{-6}$), c_2 ($\pm\delta c_2$) = 1.10×10^{-7} ($\pm 8.70 \times 10^{-9}$).

$$\delta\gamma_{\mathrm{Ref}} = \sqrt{\left[a_1^2 \cdot \exp\left(-\frac{2j(O^1D)}{b_1}\right)\right]\left[\left(\frac{\delta a_1}{a_1}\right)^2 + \left(\frac{j(O^1D)\cdot\delta b_1}{b_1^2}\right)^2\right] + (\delta c_1)^2} \quad \text{(S13)}$$

$$\delta\gamma_{\mathrm{Rea}} = \sqrt{\left[a_2^2 \cdot \exp\left(-\frac{2j(O^1D)}{b_2}\right)\right]\left[\left(\frac{\delta a_2}{a_2}\right)^2 + \left(\frac{j(O^1D)\cdot\delta b_2}{b_2^2}\right)^2\right] + (\delta c_2)^2} \quad \text{(S14)}$$

$$\mathrm{Unc}_{\gamma_{\mathrm{Ref}}} = \frac{\delta\gamma_{\mathrm{Ref}}}{\gamma_{\mathrm{Ref}}} \quad \text{(S15)}$$

$$\mathrm{Unc}_{\gamma_{\mathrm{Rea}}} = \frac{\delta\gamma_{\mathrm{Rea}}}{\gamma_{\mathrm{Rea}}} \quad \text{(S16)}$$

4. According to experimental measurement, the UV transmittance of the reaction chamber is 96%, and the UV transmittance of the reference chamber is 5%. However, we do not consider the blocking effect of the system on UV when calculating Mea-OPR, i.e., $\varphi_{\mathrm{trans}} = 1$, and the corresponding absolute uncertainty is -9%. The uncertainty of this item can be calculated using Eq. (S17).

$$\mathrm{Unc}_{\varphi_{\mathrm{trans}}} = \frac{\delta\varphi_{\mathrm{trans}}}{\varphi_{\mathrm{trans}}} = \frac{9\%}{1} = 9\% \quad \text{(S17)}$$

5. During the 1-week HONO production experiment, ΔHONO was found to have a negligible effect on Mea-OPR, so we do not consider the correction of HONO production, i.e., $\varphi_{\Delta\mathrm{HONO}} = 1$, and the corresponding absolute uncertainty is at most +4.5%. The uncertainty of this item can be calculated using Eq. (S18).

$$\mathrm{Unc}_{\varphi_{\Delta\mathrm{HONO}}} = \frac{\delta\varphi_{\Delta\mathrm{HONO}}}{\varphi_{\Delta\mathrm{HONO}}} = \frac{4.5\%}{1} = 4.5\% \quad \text{(S18)}$$

Mea-OPR can be further divided into three parts: A, B and C, wherein

$$A = \frac{\Delta NO_2 + \Delta O_3}{\tau} \quad \text{(S19)}$$

$$B = \frac{(\gamma_{Rea} \cdot \omega_{Rea} - \gamma_{Ref} \cdot \omega_{Ref}) \cdot O_{3,amb}}{D} \quad \text{(S20)}$$

$$C = \varphi_{trans} \cdot \varphi_{\Delta HONO} \quad \text{(S21)}$$

$$\delta A = \frac{\Delta NO_2 + \Delta O_3}{\tau} \cdot \sqrt{\frac{(\delta \Delta NO_2)^2 + (\delta \Delta O_3)^2}{(\Delta NO_2 + \Delta O_3)^2} + (\frac{\delta \tau}{\tau})^2} \quad \text{(S22)}$$

$$\delta B = \frac{\sqrt{(\delta \gamma_{Rea} \cdot \omega_{Rea})^2 + (\delta \gamma_{Ref} \cdot \omega_{Ref})^2} \cdot O_{3,amb}}{D} \quad \text{(S23)}$$

$$\delta C = \varphi_{trans} \cdot \varphi_{\Delta HONO} \cdot \sqrt{(\frac{\delta \varphi_{trans}}{\varphi_{trans}})^2 + (\frac{\delta \varphi_{\Delta HONO}}{\varphi_{\Delta HONO}})^2} \quad \text{(S24)}$$

Since $\text{Mea-OPR} = \frac{A + B}{C}$, the uncertainty of Mea-OPR can be calculated using Eq. (S25) and (S26) as follow:

$$\delta \text{Mea-OPR} = \frac{A + B}{C} \cdot \sqrt{\frac{(\delta A)^2 + (\delta B)^2}{(A + B)^2} + (\frac{\delta C}{C})^2} \quad \text{(S25)}$$

$$Unc_{\text{Mea-OPR}} = \frac{\delta \text{Mea-OPR}}{\text{Mea-OPR}} = \sqrt{\frac{(\delta A)^2 + (\delta B)^2}{(A + B)^2} + (\frac{\delta C}{C})^2} \quad \text{(S26)}$$

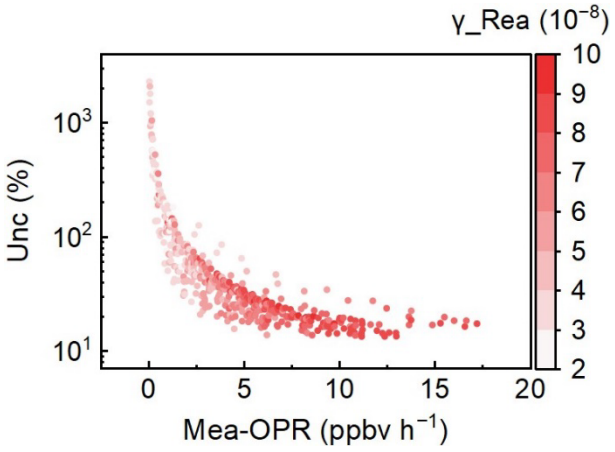

Figure S8: Total uncertainty of Mea-OPR system under different Mea-OPR. Color represents O_3 uptake coefficient in reaction chamber. Clearly, under the same Mea-OPR, when O_3 uptake coefficient decreases, corresponding uncertainty also reduces. This result further indicates the importance of reducing O_3 uptake in chambers for accurate measurement of Mea-OPR.

Table S4. Uncertainties of Mea-OPR system.

Source		Value	Uncertainty
UV transmittance	Ref	5%	−5%
	Rea	96%	−4%
Gas residence time		19.9 (±0.09) min	±0.45%
Measurement of ΔO_x	ΔNO_2		±3.8%*
	ΔO_3		±1.1%*
γ_{O3}	Ref		±4.4%*
	Rea		±23%*
γ_{NO2}			–
HONO production			+4.5%*
Total			±27%*

*Uncertainties of Mea-OPR evaluated during daytime. Total uncertainty represents the average uncertainty when Mea-OPR is above the detection limit (2.8 ppbv h^{-1}).

References

Baier, B. C., Brune, W. H., Lefer, B. L., Miller, D. O., and Martins, D. K.: Direct ozone production rate measurements and their use in assessing ozone source and receptor regions for Houston in 2013, Atmos. Environ., 114, 83–91, https://doi.org/10/gnxf26, 2015.

Sadanaga, Y., Kawasaki, S., Tanaka, Y., Kajii, Y., and Bandow, H.: New system for measuring the photochemical ozone production rate in the atmosphere, Environ. Sci. Technol., 51, 2871–2878, https://doi.org/10/f9qw59, 2017.

Saunders, S. M., Jenkin, M. E., Derwent, R. G., and Pilling, M. J.: Protocol for the development of the Master Chemical Mechanism, MCM v3 (Part A): tropospheric degradation of non-aromatic volatile organic compounds, Atmos. Chem. Phys., 3, 161–180, https://doi.org/10.5194/acp-3-161-2003, 2003.

Sklaveniti, S., Locoge, N., Stevens, P. S., Wood, E., Kundu, S., and Dusanter, S.: Development of an instrument for direct ozone production rate measurements: measurement reliability and current limitations, Atmos. Meas. Tech., 11, 741–761, https://doi.org/10/gmttxc, 2018.

Wang, Y., Wang, J., Wang, Y., Zhang, Y., Woodward-Massey, R., Zhang, C., Kuang, Y., Zhu, J., Shang, J., Li, X., Zeng, L., Lin, W., and Ye, C.: Experimental and kinetic model evaluation of HONO production from surface nitrate photolysis, Atmos. Environ., 296, 119568, https://doi.org/10.1016/j.atmosenv.2022.119568, 2023.

Wei, N., Fang, B., Zhao, W., Wang, C., Yang, N., Zhang, W., Chen, W., and Fittschen, C.: Time-Resolved Laser-Flash Photolysis Faraday Rotation Spectrometer: A new tool for total OH reactivity measurement and free radical kinetics research, Anal. Chem., 92, 4334–4339, https://doi.org/10.1021/acs.analchem.9b05117, 2020.

Zhou, X., Gao, H., He, Y., Huang, G., Bertman, S. B., Civerolo, K., and Schwab, J.: Nitric acid photolysis on surfaces in low-NO_x environments: Significant atmospheric implications, Geophys. Res. Lett., 30, n/a-n/a, https://doi.org/10.1029/2003GL018620, 2003.